CHARACTERIZATION OF BUBBLING FLUIDIZATION REGIME BY ANALYSIS OF PRESSURE FLUCTUATIONS

Xiang Jie, Li Qinghai, Zhang Yanguo*

Key Laboratory for Thermal Science and Power Engineering of Ministry of Education, Department of Thermal Engineering, Tsinghua University, Beijing 100084, China

*Email: *zhangyg@tsinghua.edu.cn*

Abstract – Statistical, power spectral and chaos analysis methods were used to analyze pressure fluctuations in a bubbling fluidized bed. The effects of superficial gas velocity, static bed height, particle size and position of pressure probe on the flow behavior were investigated. For the bubbling fluidized bed in this work, the flow regime can be further divided into three subregions. The flow behavior in terms of Kolmogorov entropy at the bottom of the bed was more complex than that at the upper part of the bed. Kolmogorov entropy decreased with increasing static bed height. The amplitude of pressure fluctuations increased with the superficial gas velocity and the static bed height. The dominant frequency of pressure fluctuations in the bed decreased with the static bed height and was independent of axial position of the pressure tap and particle size as gas velocity reached a certain value.

INTRODUCTION

Gas-solid fluidized beds are widely used in industrial processes (Kunii and Levenspiel, 1991). Their performances strongly depend on the flow dynamics. Nonlinear particle-particle and particle-gas interactions lead to complex flow behavior of the gas-solid two-phase flow. The characteristics of the gas-solid flow are influenced by many factors. Geldart (1973) classified particles into four groups (A, B, C and D). Particles in each group have similar fluidizing characteristics, but particles within the same group can reach different types of fluidization regimes with increasing superficial gas velocity (U_g).

Researchers (e.g. Grace, 1986; Li and Kwauk, 1980; Yerushalmi and Cankurt, 1979) have proposed various two dimensional diagrams to predict the flow regime under different conditions. Grace (1986) proposed a simple and clear flow regime diagram using dimensionless particle size and superficial gas velocity, which is more useful for engineering practice. However, in the diagram, each typical flow regime is mapped onto a region, covering a relatively wide range of particle diameters and gas velocities. When a more specific description of the flow behavior is needed, each typical flow regime should be further divided into smaller regions with more details.

Quantitative description of flow dynamics in a fluidized bed can be obtained from the analysis of fluctuating signals, such as pressure fluctuations and local solids concentration fluctuations. Pressure is often chosen because it is a significant indicator of dynamics of gas-solid fluidized beds and easy to measure even under industrial conditions (Bi, 2007; van Ommen et al., 2011). On the other hand, it is complicated to obtain useful information from pressure fluctuations and then interpret the results (van Ommen et al., 2011). Early studies on pressure fluctuations in gas-solid fluidized beds mainly focused on the oscillating phenomena in the bed. Several models have been proposed to predict the dominant frequency (Baskakov et al., 1986; Verloop and Heertjes, 1974; Hiby, 1967). Among the early researchers who studied pressure fluctuation, Fan et al. (1981) investigated the causes of pressure fluctuations and the effects of gas velocity, bed height, particle size and distributor design on the dominant frequency and amplitude of the fluctuations. Researchers have tried various time-series analysis methods, including time domain analysis, frequency domain analysis and chaos analysis to analyze pressure fluctuations, comparison between which have been reviewed (Johnsson et al., 2000; Sasic et al., 2007; van Ommen et al., 2011).

Time domain analysis is mainly performed by statistical calculation of pressure fluctuations such as standard

deviation, skewness, kurtosis, probability density distribution. Frequency domain analysis is mainly about the analysis of the dominant frequency in lower frequencies (Kage et al., 1991) and the fall-off characteristics in higher frequencies (van der Schaaf et al., 1999) of the power spectrum as well as the analysis of signal components in different frequency ranges by wavelet transform (Zhao and Yang, 2003). Time domain analysis and frequency domain analysis are commonly used; they belong to linear analysis methods. In contrast, chaos analysis belongs to nonlinear analysis methods. Invariants of chaotic attractor, such as correlation dimension, Lyapunov exponent and Kolmogorov entropy, are applied in chaos analyses to quantify the chaotic behavior. In the 1990s, many researchers applied chaos analysis to investigate the fluctuating signals in the fluidized beds; they found that fluidized beds had the characteristics of chaotic systems. Among the invariants, Kolmogorov entropy has often been used to characterize the flow dynamics of the fluidized beds (Bai et al., 1999; Marzocchella et al., 1997; Nedeltchev et al., 2012; Schouten et al., 1996; van den Bleek et al., 2002; van den Bleek and Schouten, 1993; Zijerveld et al., 1998).

In this work we combined statistical, power spectral and chaos analysis methods to analyze the pressure fluctuations in a bubbling fluidized bed. The standard deviation, dominant frequency, Kolmogorov entropy, and the power distribution in different frequency ranges of the pressure signals were calculated. The effects of superficial gas velocity, static bed height (H_b), particle size and position of pressure probe on the flow behavior were investigated.

EXPERIMENT

The experiments were carried out in a cold fluidized bed with a cross section of 0.1 × 0.1 m^2. The schematic diagram of the experimental setup is shown in Fig. 1. The air distributor is an 8 mm thick perforated plate with 100 holes with a diameter of 1 mm. It has a 0.79% opening area. The plate was covered with a fine mesh net to prevent particles from falling into the wind box. The pressure taps were installed along the center of the wall; each of them has a fine mesh net to block the particles. Pressure in the wind box was measured through the tap at the position of P0; the other taps enabled the measurement of pressure in the bed. P1 is 2.25 cm above the distributor; P2 is 4 cm above P1. P2 through P6 are evenly spaced with an interval of 5 cm. The pressure fluctuations were measured by differential pressure transducers (CGYL-300B, with a precision of 0.25 % and a response time less than 1 ms) and a 24-bit data acquisition module (NI 9239) through a 30 cm long and 4 mm ID tube. The sampling frequency, f_s, was 1613 Hz and the sampling duration was 3 min for all cases. The fluidizing gas was ambient air supplied by a blower; the air flow rate was measured by a rotameter with a precision of 1.5 %. The pressure fluctuations at five locations P0, P1, P2, P3, and P4 were recorded. Three types of glass beads with an average particle size, d_p, of 176, 246, 354 μm, respectively, were used as bed materials. Their particle density was 2500 kg/m^3, and they belong to Group B particles. The measured minimum fluidization velocity, U_{mf}, was 0.034, 0.064, 0.125 m/s, respectively, and the voidage at U_{mf} was about 0.42 for all three types of glass beads. The gas velocities ranged from 0.07 to 0.6 m/s; the static bed height was in the range of 5- 27 cm.

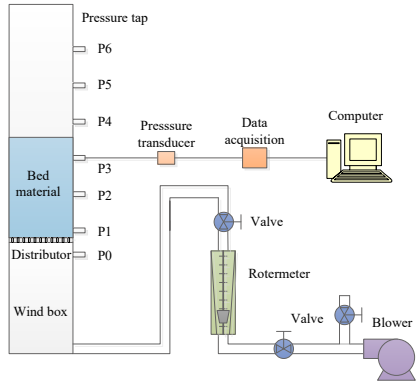

Fig. 1. Schematic diagram of the experimental setup

Power spectrum density (PSD) was estimated using Welch method (Jonhsson et al., 2000). The segment length was 20 s with an overlap of 50 %, thus there were 17 segments for a time series of 3 min and a frequency resolution of 0.5 Hz was obtained. A Hanning window was used as the window function.

Kolmogorov entropy, expressing the rate of information loss, quantifies the unpredictability of a chaotic system.

It was estimated by a maximum-likelihood approach proposed by Schouten et al. (1994a). The number of samples was set to be 20, 000 to obtain a relative standard error of 0.7 % or so. As suggested by Schouten et al. (1994b), the average cycle time was chosen as the embedding window with time delay of one time interval and the specified maximum distance was estimated by the average absolute deviation.

Discrete wavelet transform was used to analyze the power of pressure signals in different frequency ranges. The signals were decomposed up to the 10th level, using a Daubechies wavelet (db2), implemented in the Matlab. Details and approximations were reconstructed. Each detail D_k contains frequency information in the range $[f_s/2^{k+1}, f_s/2^k]$ and each approximation A_k in the range $[0, f_s/2^{k+1}]$. The variance of the signal was used as the power of the signal. The percentages of the power of both all the details and the approximation A10 to the power of the original signal were calculated.

RESULTS AND DISCUSSION

Effects of superficial gas velocity

The effects of superficial gas velocity on Kolmogorov entropy and power distribution in different frequency ranges are shown in Fig. 2. According to the behavior of bubbles, the entire process can be divided into three regions as depicted in Fig. 2a. Region 1 corresponds to locally fluidized state ($1 < U_g/U_{mf} < 1.4$), Region 2 is fully fluidized with low U_g ($1.4 < U_g/U_{mf} < 3.5$) and Region 3 is fully fluidized with relatively high U_g ($3.5 < U_g/U_{mf} < 8.7$). In Region 1, the maximum-likelihood estimates of Kolmogorov entropy (K_{ML}) at P1 and P2 increase sharply with U_g, but the effect of U_g on K_{ML} at P3 is opposite. The cause for this difference lies in the generation of a train of small bubbles at the tip of the pressure tap of P3. These small bubbles are suppressed when the influence of the bubble eruption reaches the region near P3. Therefore, the location of bubble eruption under locally fluidized state has a great impact on the pressure near the bed surface.

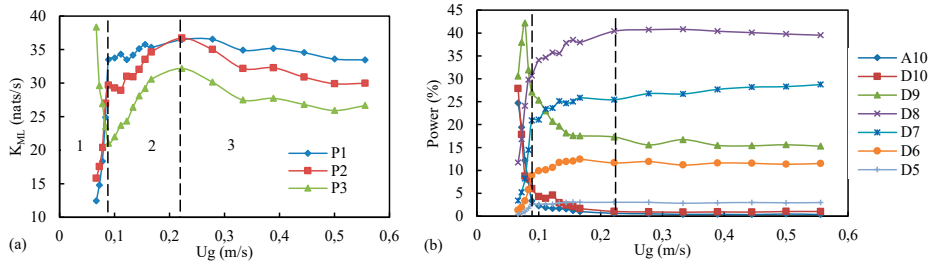

Fig. 2. Kolmogorov entropy of pressure fluctuations at different positions (a) and power of components at different levels of P1 (b) vs. superficial gas velocity (d_p = 246 μm, H_b = 13.2 cm).

In Region 2, the bed is not vigorously churned by the bubbles because the bubbles are small and their rising velocity is still low. K_{ML} increases with U_g due to the increase of both size and number of the bubbles. In Region 3, both U_g and the rising velocities of the bubbles are relatively high. The bubble can grow to the size of the bed and the bed starts churning vigorously and oscillating fiercely. As U_g increases, K_{ML} decreases slowly because the oscillation of the bed on a large scale dominates the pressure fluctuations. For the entire process, the effects of gas velocity on K_{ML} are complicated since the bubbles go through a complex process with increasing gas velocity.

As shown in Fig. 2b, with increasing U_g, the power of D6, D7 and D8 of P1 increases sharply in Region 1 followed by a moderate increase in Region 2, and only changes slightly in Region 3, which is similar to the change of K_{ML} of P1 with U_g. The majority of the power of pressure fluctuations is contained in the frequencies below 25 Hz, corresponding to the detail signals from D6 to D10 and approximation signal A10. K_{ML} and f_c of both detail and approximation signals were calculated and listed in Table 1. K_{ML} and f_c of the detail signal increase as the frequency in the detail signal increases from D10 to D1. K_{ML} and f_c of the approximation signal

first increase and then remain almost constant as the frequency in the approximation signal increases from A9 to A0, which means that K_{ML} is mainly determined by the components of frequencies below 25 Hz in the pressure fluctuations in bubbling fluidization.

In the fully fluidized bed, the closer the pressure tap to the bed surface, the smaller K_{ML} is, indicating the flow at the bottom of the bed is more complex than that near the bed surface. This can be attributed to the bubbles in terms of size and number. When it gets closer to the bed surface, the bubbles grow into fewer but larger ones, leading to simpler gas flow condition. Similar results from gauge and differential pressure in a deeper bed (H_b = 22 cm) are also obtained. For gauge pressure in Fig. 3c, except P1, K_{ML} at a lower position in the bed is greater, which is also true for differential pressure in Fig. 3d. For U_g > 0.14 m/s, K_{ML} of P2, P3 and P4 decrease slowly to a constant but K_{ML} of P1-P2, P2-P3 and P3-P4 increase to a constant. At the same position, K_{ML} of differential pressure seems to be greater than that of gauge pressure, especially at the bottom of the bed, indicating that local flow behavior is more complex than global flow behavior.

Table 1. K_{ML} and f_c of details and approximations of P1 (Ug = 0.28 m/s, d_p = 176 μm, H_b = 13 cm)

	D10	D9	D8	D7	D6	D5	D4	D3	D2	D1
K_{ML}/nats/s	3	6.1	13.1	26.1	44.9	76.9	130.6	215.6	325.4	493
f_c/Hz	1.6	3.1	5.1	9.6	18.4	36.4	74.2	155.8	337.5	671.6
	A9	A8	A7	A6	A5	A4	A3	A2	A1	A0
K_{ML}/nats/s	4.2	7.0	15.6	31.1	39.4	40.7	39.4	38.5	38.2	37.8
f_c/Hz	1.3	3.0	4.4	6.3	8.1	9.0	9.0	8.6	8.5	8.4

As shown in Fig. 3a, b, the amplitudes of both gauge and differential pressure increase with U_g because the bubbles grow larger and the bed oscillates more fiercely as U_g increases. Gauge pressure reflects both local bubble behavior and bubble behavior at other locations in the bed; differential pressure mainly reflects the bubble behavior between the two pressure taps. The amplitude of gauge pressure at the bottom of the bed is mainly dominated by the oscillation of bed materials above the pressure tap; the amplitude of gauge pressure near the bed surface and the amplitude of differential pressure are mainly dominated by the passage of bubbles. Therefore, the amplitudes of P1, P2 and P3 are close (Fig. 3a), but the amplitude of differential pressure is greater at a higher position as the bubble grows in size while rising up (Fig. 3b).

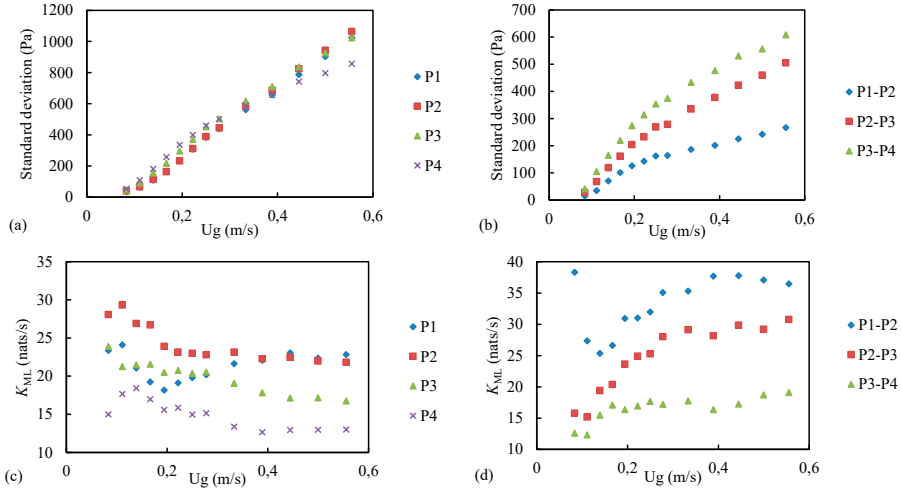

Fig. 3. Standard deviation and K_{ML} of gauge and differential pressure fluctuations at different positions vs. superficial gas velocity (d_p = 246 μm, H_b = 22 cm).

Dominant frequency

In Fig. 4a, after U_g exceeds 0.28 m/s, the dominant frequencies, corresponding to the maximum PSD, of pressures at all axial positions almost coincide. This is the dominant influence of bed oscillation across the whole bed caused by bubble passage and bubble eruption at the bed surface. Fig. 4b shows the dominant frequencies of P1 with increasing U_g at different static bed heights. It is shown that the dominant frequency decreases with increasing H_b, for bubble grows larger in a deeper bed, resulting in a lower frequency. As U_g increases, the dominant frequency tends to decrease slightly. As shown in Fig. 4c, for Ug ≥ 0.33 m/s, the dominant frequencies of P1 for three different particle sizes at the same H_b of 18 cm are close, indicating the small dependence of dominant frequency on particle size.

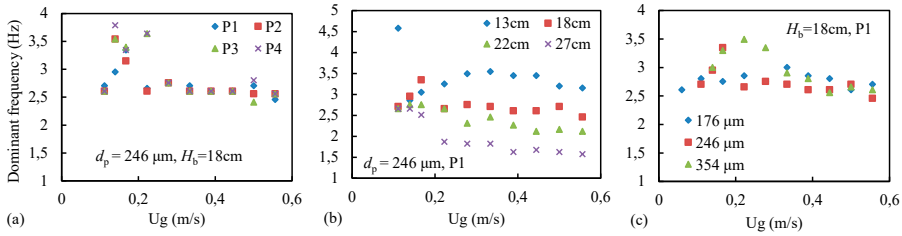

Fig. 4. Dominant frequency of pressure fluctuations at different positions (a), for different static bed height (b), and for different particle sizes (c) vs. superficial gas velocity.

Effects of static bed height

As shown in Fig. 5a, for almost all of gas velocities, as H_b increases, K_{ML} decreases and the decrement of K_{ML} decreases too. The effects of H_b on the flow is mainly reflected by its influence on the bubble size. Before reaching the minimum slugging bed height, the maximum bubble size in the bed increases with H_b. According to the analysis of Johnsson et al. (2000), K_{ML} is related to the complexity of the macro-structure of the flow, and it decreases with the reduced complexity of the macro-structure. The more complex is the flow, the smaller the time scale of the macro-structure is, and the higher the average cycle frequency becomes. As the bubbles grow in size, the complexity of the macro-structure decreases so that the dominant frequency decreases. Consequently, as H_b increases, the complexity of the flow decreases and K_{ML} decreases. However, when U_g > 0.28 m/s, K_{ML} of P3 at H_b of 22 and 27 cm are almost the same (Fig. 5b), which is also shown in Fig. 6c that K_{ML} of P3 and P4 nearly remains unchanged when H_b exceeding 22 cm.

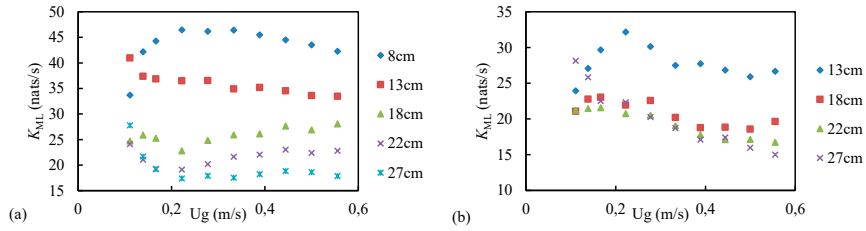

Fig. 5. K_{ML} vs. superficial gas velocity at different static bed heights. (a): P1, (b): P3. d_p = 246 μm.

As H_b increases from 5 to 25 cm with an increment of 1 cm, the bed surface passes the pressure taps successively (Table 2). Relative to the bed surface, the position of each pressure tap is classified into three types: above the bed surface, just below the bed surface and well below the bed surface. As shown in Fig. 6a, the average pressure increases linearly with H_b after the bed surface exceeds the pressure tap.

As H_b increases, the maximum size of the bubbles increases too, resulting in an increase in amplitude of

pressure fluctuation at all positions (Fig. 6b). When H_b reaches 10 cm or so, the amplitude of P2 exceeds that of P1, and then they keep close to each other as U_g increases. When H_b reaches about 16cm, the amplitude of P3 exceeds P2. When H_b reaches about 21 cm, the amplitude of P4 exceeds P3. The amplitude of pressure is related to the bubble size passing by the pressure tap and the amount of bed materials involved in the oscillation above the pressure tap. For relatively low U_g, the impact of bubble passage on the amplitude of pressure is greater than that of the oscillation of the bed. Therefore, when the bed surface is well above the pressure tap, the bubble at a higher position is larger in size, resulting in a greater amplitude.

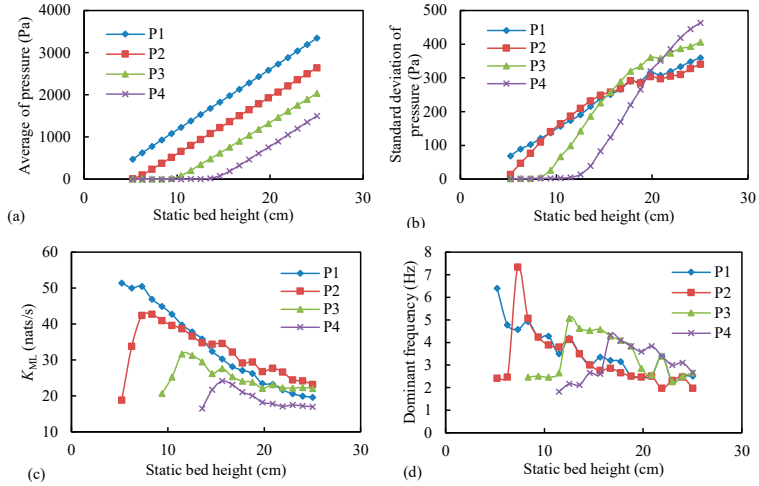

Fig. 6. Effects of static bed height on the average (a), amplitude (b), K_{ML} (c) and dominant frequency (d) of pressure fluctuations at different positions (U_g = 0.22 m/s, d_p = 246 μm).

As shown in Fig. 6c, K_{ML} of P1 decreases monotonically with H_b; however, for P2, P3, and P4, K_{ML} first increases to a maximum followed by a decreasing trend. For H_b more than 22cm, K_{ML} of P3 and P4 remain nearly constant. The measured K_{ML} values depend on the position of pressure tap, and the relative size of K_{ML} at different axial positions changes with H_b. When H_b exceeds 14 cm, K_{ML} of P2 is greater than that of P1; When H_b exceeds 21 cm, K_{ML} of P3 exceeds P1. After the bed surface is well above the position of the pressure tap, the dominant frequencies of the pressure at four axial locations tend to decrease with H_b (Fig. 6d), which concurs the results shown in Fig. 4b.

Table 2. The static bed heights, average pressure and standard deviations of pressure when the bed surface exceeds for the first time the position of pressure tap of P2, P3 and P4.

	P2	P3	P4
Position of pressure tap/cm	6.25	11.25	16.25
Static bed height/cm	5.2	9.4	13.6
Average of pressure/Pa	10.8	17.5	20.7
Standard deviation/Pa	13.5	26.2	38.6

Fig. 7 shows the power of detail and approximation signals of P1, P2 and P3 with the static bed height. For all values of H_b, the pressure tap of P1 is well below the bed surface. The static bed heights where the three types of the position of the pressure tap of P2 and P3 are demarcated are depicted as dashed lines in Fig. 7. When the pressure tap is well below the bed surface, for pressure at all positions, the power of D5, D6 and D7, corresponding to higher frequencies, decreases with H_b, the power of D8, increases to the maximum followed by a decrease with H_b, and the power of D9 and D10, corresponding to lower frequencies, increases with H_b. This accounts for the decrease of K_{ML} with H_b when the pressure tap is well below the bed surface (Fig. 7c).

When the pressure tap is just below the bed surface, the power of D6 and D7 increases with H_b and the power of D9, D10 and A10 decreases with H_b. As shown in Fig. 7d, the high frequency noises dominate the power of the pressure when the pressure tap is above the bed surface, but decrease sharply to near zero when the bed surface exceeds the pressure tap.

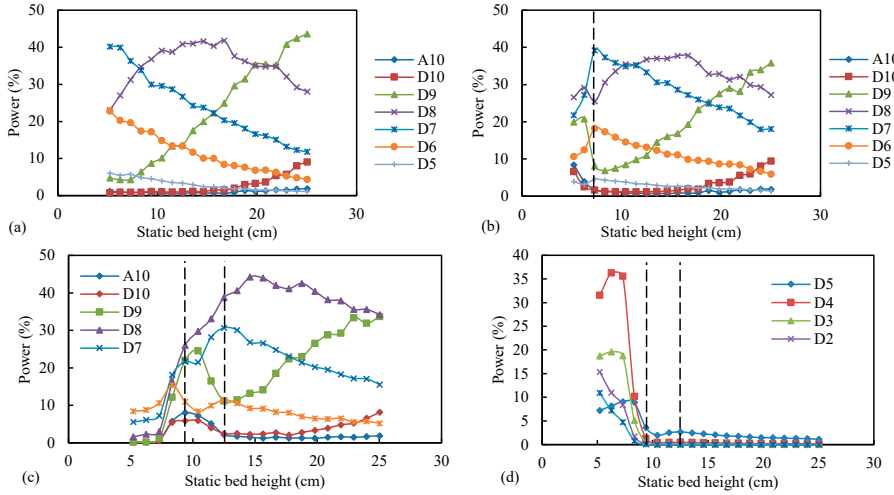

Fig. 7. The power of components at different levels of P1 (a), P2 (b) and P3 (c, d) vs. static bed height. U_g = 0.22 m/s, d_p = 246 μm.

CONCLUSION

For the bubbling fluidized bed in this work, the flow regime can be further divided into three subregions. Kolmogorov entropy is mainly determined by the components of frequencies below 25 Hz in the pressure fluctuations in bubbling fluidization. The flow behavior in terms of Kolmogorov entropy at the bottom of the bed was more complex than that at the upper part of the bed. At the same position, Kolmogorov entropy of differential pressure was larger than that of gauge pressure at the bottom of the bed. Kolmogorov entropy decreased with increasing static bed height. The amplitude of pressure fluctuations was mainly dominated by bubble passage and the oscillation of the bed materials and it increased with the superficial gas velocity and the static bed height. The dominant frequency of pressure fluctuations in the bed decreased with the static bed height and was independent of axial position of the pressure tap and particle size when the gas velocity reached a certain value. The change of power distribution in different frequency ranges by wavelet analysis can be used to aid the understanding of the changes of Kolmogorov entropy and dominant frequency.

NOTATION

d_p average particle size, μm
f_s sampling frequency, Hz
H_b static bed height, cm
U_g superficial gas velocity, m/s
K_{ML} maximum-likelihood estimate of Kolmogorov entropy, nats/s
U_{mf} minimum fluidization velocity, m/s

ACKNOWLEDGEMENTS

This work was supported by National Science Foundation of China (No. 21376134).

REFERENCES

Bai, D., Issangya, A.S., Grace, J.R., 1999. Characteristics of Gas-Fluidized Beds in Different Flow Regimes. Industrial & Engineering Chemistry Research 38,(3), 803-811.

Baskakov, A.P., Tuponogov, V.G., Filippovsky, N.F., 1986. A study of pressure fluctuations in a bubbling fluidized bed. Powder Technology 45,(2), 113-117.

Bi, H.T., 2007. A critical review of the complex pressure fluctuation phenomenon in gas-solids fluidized beds. Chemical Engineering Science 62,(13), 3473-3493.

Fan, L.T., Ho, T.C., Hiraoka, S., Walawender, W.P., 1981. Pressure fluctuations in a fluidized bed. AIChE Journal 27,(3), 388-396.

Geldart, D., 1973. Types of gas fluidization. Powder Technology 7,(5), 285-292.

Grace, J.R., 1986. Contacting modes and behaviour classification of gas—solid and other two-phase suspensions. The Canadian Journal of Chemical Engineering 64,(3), 353-363.

Hiby, J.W., 1967. Periodic phenomena connected with gas–solid fluidization. In: Proceedings of the International Symposium on Fluidization. Netherlands University Press, Amsterdam, pp. 99–112.

Johnsson, F., Zijerveld, R.C., Schouten, J.C., van den Bleek, C.M., Leckner, B., 2000. Characterization of fluidization regimes by time-series analysis of pressure fluctuations. International Journal of Multiphase Flow 26,(4), 663-715.

Kage, H., Iwasaki, N., Yamaguchi, H., Matsuno, Y., 1991. Frequency analysis of pressure fluctuation in fluidized bed plenum. Journal of Chemical Engineering of Japan 24,(1), 76-81.

Kunii, D., Levenspiel, O., 1991. Fluidization engineering, 2nd ed. Butterworth-Heinemann, Boston.

Li, Y., Kwauk, M., 1980. The dynamics of fast fluidization. In: Grace, J.R., Matsen, J.M. (Eds.), Fluidization. Plenum Press, New York and London, pp.537-544.

Marzocchella, A., Zijerveld, R.C., Schouten, J.C., van den Bleek, C.M., 1997. Chaotic behavior of gas-solids flow in the riser of a laboratory-scale circulating fluidized bed. AIChE Journal 43,(6), 1458-1468.

Nedeltchev, S., Aradhya, S., Zaid, F., Al-Dahhan, M., 2012. Flow Regime Identification in Three Multiphase Reactors Based on Kolmogorov Entropies Derived from Gauge Pressure Fluctuations. Journal of Chemical Engineering of Japan 45,(9), 757-764.

Sasic, S., Leckner, B., Johnsson, F., 2007. Characterization of fluid dynamics of fluidized beds by analysis of pressure fluctuations. Progress in Energy and Combustion Science 33,(5), 453-496.

Schouten, J.C., Takens, F., van den Bleek, C.M., 1994b. Estimation of the dimension of a noisy attractor. Physical Review E 50,(3), 1851-1861.

Schouten, J.C., Takens, F., van den Bleek, C.M., 1994a. Maximum-likelihood estimation of the entropy of an attractor. Physical Review E 49,(1), 126-129.

Schouten, J.C., Vander Stappen, M.L.M., van den Bleek, C.M., 1996. Scale-up of chaotic fluidized bed hydrodynamics. Chemical Engineering Science 51,(10), 1991-2000.

van den Bleek, C.M., Coppens, M.O., Schouten, J.C., 2002. Application of chaos analysis to multiphase reactors. Chemical Engineering Science 57,(22), 4763-4778.

van den Bleek, C.M., Schouten, J.C., 1993. Deterministic chaos: a new tool in fluidized bed design and operation. Chemical Engineering Journal & the Biochemical Engineering Journal 53,(1), 75-87.

van der Schaaf, J., Johnsson, F., Schouten, J.C., van den Bleek, C.M., 1999. Fourier analysis of nonlinear pressure fluctuations in gas-solids flow in CFB risers – Observing solids structures and gas/particle turbulence. Chemical Engineering Science 54,(22), 5541-5546.

van Ommen, J.R. et al., 2011. Time-series analysis of pressure fluctuations in gas-solid fluidized beds - A review. International Journal of Multiphase Flow 37,(5), 403-428.

Verloop, J., Heertjes, P.M., 1974. Periodic pressure fluctuations in fluidized beds. Chemical Engineering Science 29,(4), 1035-1042.

Yerushalmi, J., Cankurt, N.T., 1979. Further studies of the regimes of fluidization. Powder Technology 24,(2), 187-205.

Zhao, G.B., Yang, Y.R., 2003. Multiscale resolution of fluidized-bed pressure fluctuations. AIChE Journal 49,(4), 869-882.

Zijerveld, R.C., Johnsson, F., Marzocchella, A., Schouten, J.C., van den Bleek, C.M., 1998. Fluidization regimes and transitions from fixed bed to dilute transport flow. Powder Technology 95,(3), 185-204.